

RESEARCH

Open Access



Xeno-free induced pluripotent stem cell-derived neural progenitor cells for in vivo applications

Ruslan Rust^{1*} , Rebecca Z. Weber^{1,2} , Melanie Generali¹ , Debora Kehl¹, Chantal Bodenmann¹, Daniela Uhr¹, Debora Wanner¹, Kathrin J. Zürcher¹, Hirohide Saito⁴ , Simon P. Hoerstrup^{1,3}, Roger M. Nitsch^{1,2} and Christian Tackenberg^{1,2*} 

Abstract

Background: Currently, there is no regenerative therapy for patients with neurological and neurodegenerative disorders. Cell-therapies have emerged as a potential treatment for numerous brain diseases. Despite recent advances in stem cell technology, major concerns have been raised regarding the feasibility and safety of cell therapies for clinical applications.

Methods: We generated good manufacturing practice (GMP)-compatible neural progenitor cells (NPCs) from transgene- and xeno-free induced pluripotent stem cells (iPSCs) that can be smoothly adapted for clinical applications. NPCs were characterized in vitro for their differentiation potential and in vivo after transplantation into wild type as well as genetically immunosuppressed mice.

Results: Generated NPCs had a stable gene-expression over at least 15 passages and could be scaled for up to 10^{18} cells per initially seeded 10^6 cells. After withdrawal of growth factors in vitro, cells adapted a neural fate and mainly differentiated into active neurons. To ensure a pure NPC population for in vivo applications, we reduced the risk of iPSC contamination by applying micro RNA-switch technology as a safety checkpoint. Using lentiviral transduction with a fluorescent and bioluminescent dual-reporter construct, combined with non-invasive in vivo bioluminescent imaging, we longitudinally tracked the grafted cells in healthy wild-type and genetically immunosuppressed mice as well as in a mouse model of ischemic stroke. Long term in-depth characterization revealed that transplanted NPCs have the capability to survive and spontaneously differentiate into functional and mature neurons throughout a time course of a month, while no residual pluripotent cells were detectable.

Conclusion: We describe the generation of transgene- and xeno-free NPCs. This simple differentiation protocol combined with the ability of in vivo cell tracking presents a valuable tool to develop safe and effective cell therapies for various brain injuries.

Keywords: NPCs, Neural stem cells, iPSCs, Cell therapy, Intraparenchymal transplantation, Bioluminescence imaging, In vivo imaging, Clinical application, Regeneration, Stroke, Brain injury, Cell transplantation

Background

Neurodegenerative diseases and other brain injuries represent a huge personal and economic burden [1]. Cell-based therapy is considered an emerging treatment paradigm which has the potential to regenerate damaged

*Correspondence: ruslan.rust@irem.uzh.ch; christian.tackenberg@irem.uzh.ch

¹ Institute for Regenerative Medicine, University of Zurich, Wagistrasse 12, 8952 Schlieren, Switzerland
Full list of author information is available at the end of the article



© The Author(s) 2022, corrected publication 2022. **Open Access** This article is licensed under a Creative Commons Attribution 4.0 International License, which permits use, sharing, adaptation, distribution and reproduction in any medium or format, as long as you give appropriate credit to the original author(s) and the source, provide a link to the Creative Commons licence, and indicate if changes were made. The images or other third party material in this article are included in the article's Creative Commons licence, unless indicated otherwise in a credit line to the material. If material is not included in the article's Creative Commons licence and your intended use is not permitted by statutory regulation or exceeds the permitted use, you will need to obtain permission directly from the copyright holder. To view a copy of this licence, visit <http://creativecommons.org/licenses/by/4.0/>. The Creative Commons Public Domain Dedication waiver (<http://creativecommons.org/publicdomain/zero/1.0/>) applies to the data made available in this article, unless otherwise stated in a credit line to the data.

tissue and restore brain function. While safety and feasibility of administering different types of stem cell therapies seem to be reasonably proven, its efficacy remains uncertain due to conflicting results in clinical trials [2]. A major limitation in a clinical set-up is the choice of a reliable and scalable cell source as dosing of up to 1 billion cells may be required for a single transplantation [3]. Most clinical trials rely on the use of primary mesenchymal stem cells (MSCs) due to their ubiquitous presence in the adult body. However, MSCs have major drawbacks with regard to heterogeneity, scalability and differentiation potential, especially into cell types of the neural lineage. Recent developments in induced pluripotent stem cell (iPSC) technology facilitated the infinite generation of neural progenitor cells (NPCs), a more homogenous cell source for brain regeneration through cell replacement, neuroprotection and/or immunomodulation [4].

While advancing the iPSC technology towards clinical reality, challenges have emerged regarding the presence of transgenes following reprogramming, xenogenic factors in culture media and the risk of teratoma formation from undifferentiated cells in graft recipients [5].

The use of the non-integrative RNA Sendai virus vector enabled reprogramming free of vector and transgene sequences [6]. Moreover, improved protocols for NPC differentiation and culture enabled propagation in defined media omitting xenogenic factors [7]. The risk of teratoma formation can be reduced by applying highly efficient differentiation protocols and/or effective purification techniques, such as the RNA Switch technology to specifically eliminate pluripotent residuals from cultures [8, 9]. This technique is based on the presence of cell-specific micro RNA (miRNA), that can be used to either enrich or eliminate a specific cell type from a cell culture. These advancements increased the safety and feasibility of NPCs for preclinical and clinical in vivo applications. However, there is still poor understanding of the spatiotemporal kinetics, survival capabilities and differentiation phenotype of transplanted cells in an in vivo system that need to be answered before translating cell therapies into standard clinical applications.

Here, we generated and characterized NPCs from iPSCs without genomic modification and under a xenon-free, chemically defined environment. The generated NPCs showed a stable gene expression over 15 passages and capability to spontaneously differentiate into functionally active neurons in vitro. We further ensured a pure NPCs population by eliminating residual iPSCs using RNA-switch technology. To characterize the fate of NPCs in vivo, cells were transduced using a dual-reporter

system consisting of bioluminescence and fluorescence reporters. Transplanted grafts were longitudinally tracked and phenotyped 1 month after transplantation. The differentiation profile of NPCs revealed a strong preference to the neuronal fate with the expression of various neuronal markers. On the basis of the analysis in this study, we demonstrate the reliable generation of highly pure NPCs with a reduced risk of pluripotent residuals for long-term in vivo applications in the mouse.

Methods

Generation and maintenance of NPCs

NPCs were generated as previously described [10] with modifications. In detail, 80,000 iPSCs per well were plated on day - 2 on a 12-well plate, coated with Vitronectin (StemMACS iPS-Brew XF (Miltenyi), supplemented with 2µM Thiazovivin) and incubated overnight.

On day - 1, cells were washed once in PBS and the medium was changed to fresh StemMACS iPS-Brew XF.

On day 0, NPC differentiation was induced by washing cells in PBS and changing medium to Neural Induction Medium 1 (50% DMEM/F12, 50% Neurobasal medium, 1 × N2-supplement, 1 × B27-supplement, 1 × Glutamax, 10 ng/ml hLIF, 4 µM CHIR99021, 3 µM SB431542, 2 µM Dorsomorphin, 0.1 µM Compound E). On day 1 fresh medium was added. On day 2 cells were washed with PBS and the medium was changed to Neural Induction Medium 2 (50% DMEM/F12, 50% Neurobasal medium, 1 × N2-supplement, 1 × B27-supplement, 1 × Glutamax, 10 ng/ml hLIF, 4 µM CHIR99021, 3 µM SB431542, 0.1 µM Compound E) followed by medium change every day for 4 days. On day 6 cells were split onto pLO/L521-coated plates in Neural Stem cell Maintenance Medium (NSMM, 50% DMEM/F12, 50% Neurobasal medium, 1 × N2-supplement, 1 × B27-supplement, 1 × Glutamax, 10 ng/ml hLIF, 4 µM CHIR99021, 3 µM SB431542).

NSMM medium was changed every day and cells were split when reaching 80–100% confluency. For the first 6 passages 2 µM Thiazovivin was added after splitting. From passage 2 on NSMM medium was supplemented with 5 ng/ml FGF2. See further details for media and cell culture materials in Additional file 8: Table S1.

Neural differentiation of NPCs

NPCs were seeded 200'000 cells/ml in NSMM + 5 ng/ml FGF2 on 24-well plates. Differentiation was induced by withdrawal of small molecules CHIR99021, SB431542, hLIF and FGF2. Cells were cultured for 21 days in NSMM without small molecules, hLIF and FGF2 with daily media changes during the first week and media changes every other day or biweekly in the second or third week, respectively.

NPC transduction for in vivo tracking

For in vivo cell tracking, dual-reporter lentiviral plasmids pLL410_EF1a-rFLuc-T2A-GFP-mPGK-Puro (LL410PA-1) and pLL-CMV-rFLuc-T2A-GFP-mPGK-Puro (LL310PA-1) were obtained from System Bioscience. Lentiviral generation was carried out as previously described [11]. For NPC transduction, 650'000 cells/well were seeded in NSMM+5 ng/ml FGF2. After 24 h, 20 μ l virus per well was added during medium change (= 1/100 virus per well).

NPC transduction and calcium imaging

Adeno-associated viruses (AAV) at titer $\geq 1 \times 10^{13}$ vg/ml, expressing mRuby2 and GCaMP6s under the human synapsin promoter (pAAV-hSyn1-mRuby2-GSG-P2A-GCaMP6s-WPRE-pA) was purchased from Addgene (50,942-AAV1). NPCs were differentiated to neural cells as described above and transduced by adding 1.44 μ l virus solution per well in a μ -Slide 4 Well 5 days after cell seeding. For neuronal stimulation KCl was added during imaging to a final concentration of 60 mM.

Images were acquired using Leica SP8 confocal microscope, equipped with 10 \times HC PL FLUOTAR 0.30 DRY objective. Image settings for GCaMP6s were the following: 488 nm laser excitation (Argon laser); xyt scan mode; 512 \times 512 pixel; 15 min time-lapse imaging with 1.29 s intervals; 200 Hz. Image settings for mRuby were the following: 561 nm laser excitation (DPSS); xyz scan mode; 1024 \times 1024 pixel; 100 Hz.

Image quantification for mRuby and GCaMP6

For mRuby quantification, fluorescence signal intensity of mRuby was measured in randomly selected regions of interest (ROIs) and normalized to the DAPI cell count using Fiji (ImageJ). For GCaMP6 quantification: at least 20 differentiated neural cells per condition were identified and outlined as ROIs using Fiji (ImageJ). Fluorescence signal intensity in these ROIs was continuously measured over 500 s.

qPCR

RNA extraction was carried out using Quiagen RNeasy kit according to the manufacturer's recommendations. qPCR was performed using SYBR green kit (iTaq Universal SYBR Green Supermix from Biorad) containing 0.5 μ M of each primer with the following cycling conditions (hold stage: 95 $^{\circ}$ C, 10 min, 1 cycle; PCR stage (95 $^{\circ}$ C, 15 s, 60 $^{\circ}$ C 1 min; 95 $^{\circ}$ C 15 s, 40 cycles; Melting curve (95 $^{\circ}$ C, 15 s, 60 $^{\circ}$ C, 1 min). Human total brain Total RNA (ThermoFisher, QS0611) served as a positive control (see Additional file 9: Table S2).

Immunocytochemistry

ICC was performed with 4% paraformaldehyde (PFA)/4% sucrose fixed cells, whereby donkey serum was used for blocking and staining solution. Incubation of primary antibody namely NPC specific markers Pax6, Sox1 and Nestin as well as iPSC specific marker Oct4, was performed at 4 $^{\circ}$ C overnight. The next day the secondary antibody was incubated for 2 h at room temperature (RT) followed by DAPI staining. Confocal microscopy was used for imaging.

Flow cytometry

Cells were thawed and incubated in FACS buffer (0.1% BSA in PBS) with live/dead Fixable Near-IR staining (Molecular probes) for 30 min at 4 $^{\circ}$ C. Subsequently, cells were fixed in 1% PFA for 20 min at RT and permeabilized with FACS buffer containing 0.5% Saponin for 20 min at 4 $^{\circ}$ C. Intracellular antibodies namely Pax6, Nestin, Sox1 and Oct4 were then used for staining for 30 min at 4 $^{\circ}$ C. Cells were acquired using a LSR Fortessa (BD Bioscience) and the data were analyzed by FlowJo software (Tree Star).

Karyotyping

Karyotyping of NPCs was carried out as described previously [11]. In brief, NPCs, at the relevant passages, were treated with 80 ng/ml colcemide to achieve a metaphase-arrest allowing for chromosome visualization. Cells were harvested, incubated for 15 min in 75 mM KCl and fixed for 30 min in a 3:1 mixture of methanol/acetic acid. Spreads were prepared on methanol-cleaned glass slides, dried overnight, stained for 10 min in quinacrine solution and analyzed using Zeiss Axioskop HBO 50 fluorescent microscope (Zeiss) and Ikaros Software (MetaSystems).

RNA switch

The RNA switch was prepared as previously described [8, 12]. Briefly, template DNA for in vitro transcription of normal mRNA was amplified by PCR from a vector encoding for either Barnase, Barstar, or puromycin using appropriate primers with the T7 promoter and poly(A) tail. The template of miR-302a-5p responsive OFF switch (Barstar) was amplified from the same vector by PCR using the primer containing miRNA anti-sense sequence at 5'UTR. For the miR-302a-5p responsive ON switch (Barnase), the open reading frame, poly(A) tail, and miRNA anti-sense sequence were amplified from the same vector by the first PCR. Then, the PCR product and extra sequence were fused in this order by a second PCR. All template DNAs were purified using the Min-Elute PCR Purification Kit. The RNAs were transcribed for 6h at 37 $^{\circ}$ C using MEGAScript T7 Transcription Kit

using 1-Methylpseudouridine-5'-Triphosphate and Anti Reverse Cap Analog, ARCA. The transcribed RNA was treated with Turbo DNase I and antarctic phosphatase to remove template DNA and purified by RNeasy MinElute Cleanup Kit (QIAGEN). The concentration was determined by Qubit microRNA Assay Kit.

A day before transfection, cells were passaged as detailed above and seeded onto PLO/L521 coated plates. The following day, mRNA was transfected using Lipofectamin RNAiMAX Transfection Reagent. The transfection complex was added to the cells in a drop-wise manner and the plate was agitated before being placed into the incubator, followed by a medium change after 4h. To remove non-transfected cells, a puromycin selection was carried out by treatment with 2 µg/ml puromycin for 24h. Cells were finally analysed by flow cytometry.

In vitro luciferase assay

Cells were seeded on 24-well plate and a serial diluted luciferin standard curve (starting concentration was 300 µg/ml) was made. After incubating cells for 10 min at 37 °C bioluminescence was measured with Tecan M1000 pro.

NPC viability analysis

To determine viability of NPC after thawing and before transplantation, NPCs (150,000 cells/ml in PBS) were stored on ice and cell viability was measured using the Vi-Cell XR Cell Viability Analyzer.

Animals

All animal experiments were performed in accordance with governmental and institutional (University of Zurich) guidelines and had been approved by the Cantonal Veterinary Office of Zurich (License number: 31687). Immunocompromised recombination activating gene 2 knockout mice (Rag2^{-/-}, $n=3$), non-obese diabetic SCID gamma mice (NSG, $n=4$) and wild type (wt) mice with a C57BL/6 background were used (10 – 14 weeks old, female and male, $n=10$). Animals were housed in standard Type II/III cages at least in pairs in a temperature and humidity-controlled room with a constant 12/12 h light/dark cycle (light on from 06.00 a.m. until 6:00 p.m.) and food/water ad libitum. Researchers were blinded for the cell number they injected as well as for tissue collection and analysis. No randomization was performed. Number of animals used was calculated based on previous studies [13].

Cell transplantation

Cells were transplanted as previously described [14]. In brief, NPCs at passage number ≥ 11 were used in all

experiments. At time of cell transplantation, GFP⁺/Luc⁺ NPCs were diluted with a final concentration of 8×10^4 cells/µL in sterile 1 × PBS (pH 7.4, without calcium or magnesium; Thermo Fisher Scientific) and stored on ice until transplantation. Mice were anesthetized using isoflurane (4% induction, 1.5% maintenance; Attane, Provet AG). Analgesic (Rimadyl; Pfizer) was administered subcutaneously prior to surgery (5 mg/kg body weight). Animals were placed in a stereotactic frame (David Kopf Instruments), the surgical area was sanitized, and the skull was exposed through a midline skin incision to reveal *lambda* and *bregma* points. Coordinates were calculated (the coordinates of interest chosen for this protocol were: AP: +0.5, ML: +1.5, DV: -0.8 relative to bregma) and a hole was drilled using a surgical dental drill (Foredom, Bethel CT). Mice were injected with 1.6×10^5 cells (2µL/injection) using a 10-µL Hamilton microsyringe (33-gauge) and a micropump system with a flow rate of 0.3 µL/min (injection) and 1.5 µL/min (withdrawal). In addition, serial dilutions (1.8×10^5 , 1×10^5 , 6×10^4 , 1.2×10^4 , 6×10^3) of NPCs were injected into the cortex (AP: +0.5, ML: +1.5, DV: -0.8 relative to bregma) to determine the minimum cell number that can be detected in vivo. Wounds were sealed using a 6/0 silk suture and mice were allowed to recover in cages with heating pads. For postoperative care, all animals received analgesics (Rimadyl, Pfizer) for at least 2 days after surgery. Stroke mice received NPC transplantations at 7 days after stroke induction as this time period is considered clinically more relevant and has shown to allow higher survival rates of the graft compared to acute transplantations into a hostile stroke environment [15, 16].

Photothrombotic stroke

The induction of a photothrombotic stroke was carried out as previously described in wild-type (wt) mice [14, 17–20] and in NSG and Rag2^{-/-} mice. In brief, mice were anesthetized using isoflurane (4% induction, 1.5% maintenance, Attane, Provet AG). They received analgesic (Novalgine, Sanofi) 24 h prior to the start of the procedure, administered via drinking water. A photothrombotic lesion was induced in the right sensorimotor cortex. Briefly, animals were fixed in a stereotactic frame (David Kopf Instruments) and the surgical area (from the back of the neck up to the eyes) was shaved and sanitized (Betadine, Braun). Anaesthesia was maintained using a face mask. Eye lubricant (Vitamin A, Bausch&Lomb) was applied, and body temperature was constantly kept between 36° and 37 °C using a heating pad. The skull was exposed through a midline skin incision. A cold light source (Olympus KL 1,500LCS, 150 W, 3,000 K) was positioned over the right forebrain

cortex (anterior/posterior: -1.5 – $+1.5$ mm and medial/lateral 0 mm to $+2$ mm relative to Bregma). 5 min prior to illumination, Rose Bengal (15 mg/ml, in 0.9% NaCl, Sigma) was injected intraperitoneally. Subsequently, the exposed area was illuminated through the intact skull using an opaque template with an opening of 3×4 mm. After 10.5 min, light exposure was stopped and the wound was closed using a 6/0 silk suture. For postoperative care, all animals received analgesics (Novalgine, Sanofi and Rimadyl, Zoetis) for at least 3 days after surgery.

Immunohistochemistry

For histological analysis, animals were euthanized by intraperitoneal application of pentobarbital (150 mg/kg body weight, Streuli Pharma AG) and transcardially perfused with Ringer solution (containing 5 ml/l Heparin, B. Braun) followed by PFA (4%, in 0.2 M phosphate buffer, pH 7). Brains were postfixed for approximately 4 h in the same fixative, then transferred to 30% sucrose for cryoprotection and stored at 4°C . Coronal sections with a thickness of $40\ \mu\text{m}$ were cut using a sliding microtome (Microm HM430, Leica), collected and stored as free-floating sections in cryoprotectant solution at -20°C until further processing.

Brain sections were washed with 0.1 M phosphate buffer (PB) and incubated with blocking solution containing donkey serum (5%, Sigma) in PB for 60 min at room temperature. Sections were incubated overnight at 4°C with mouse anti-nuclei antibody (Merck, 1:100) to stain for transplanted human NPCs. To identify transplanted cells at different developmental stages, the following antibodies were used: Goat anti-human NANOG (R&D systems, 1:200), rabbit Oct-4A (Cell Signaling Technology, 1:200), mouse Anti-PAX6 monoclonal antibody (Thermo Fisher Scientific, 1:200), mouse Anti-NeuN Antibody (Merck, #MAB377, 1:200), rabbit Anti-Neurofilament 200 antibody (Merck, #N4142, 1:100), rabbit Anti-BetaIII-Tubulin antibody (Abcam, #ab18207, 1:500), mouse MAP2 monoclonal antibody (Thermo Fisher Scientific, 1:100), rabbit Anti-S100b antibody (Thermo Fisher Scientific, 1:300). To identify proliferating cells, rabbit Anti-Ki67 antibody (Thermo Fisher Scientific, 1:150) was used. The primary antibody incubation was followed by 2 h incubation at room temperature with corresponding fluorescent secondary antibodies (1:500, Thermo Fisher Scientific). Nuclei were counterstained with DAPI (1:2000 in 0.1 M PB, Sigma). Sections were mounted in 0.1 M PB on Superfrost PlusTM microscope slides and embedded in Mowiol. All images were taken using a Leica SP8 laser scanning confocal microscope

equipped with 10x, 20x and 40x objectives. Images were processed using Fiji (ImageJ) and Adobe Illustrator CC.

HE staining

Coronal sections with a thickness of $40\ \mu\text{m}$ were washed with 0.1 M PBS and stained with hematoxylin/eosin (HE). For pathological observation under a light microscope (Leica SP8 laser scanning confocal microscope), two views (stroke area, contralateral area) at magnification 20x and 40x were randomly selected from each slide.

Infarct area and volume quantification

GFAP, IBA1 and DAPI staining was used to calculate infarct area and volume. Stained coronal brain sections were imaged using the Axio Scan.Z1 slidescanner; the ischemic lesion was clearly characterized as region of microglia infiltration, surrounded by GFAP⁺ cells. The infarct area was outlined using Fiji (ImageJ) on five to six coronal planes per brain (from Bregma in mm; 2, 1.5, 0.5, -0.50 , -1.5 , -2). The total infarct volume derived by multiplying the average infarct area by the distance between the sections.

In vivo bioluminescence imaging

Bioluminescence imaging (BLI) experiments were performed with the IVIS Spectrum CT (PerkinElmer) as described before [14]. For long-term experiments, animals were imaged in regular intervals starting 24 h after transplantation for up to 35 days. Animals used in the study to determine the minimal number of detectable cells were imaged only *once* 1.5 h after transplantation. 30 mg/ml D-luciferin potassium salt (PerkinElmer) was dissolved in NaCl (0.9%, B. Braun) and sterilized using a $0.22\ \mu\text{m}$ syringe filter. Luciferin was injected intraperitoneally to each animal with a final dose of 300 mg/kg body weight before isoflurane anaesthesia (4% induction, 1.5% maintenance; Attane, Provect AG). Before the first BLI recording, animals were shaved on the head region. Image acquisition was performed for 20 min under the following setting: *Field of View: A*, *Subject height: 1.5 cm*, *Binning: 16*, *F/Stop: 2*. Exposure time (ranging from 1 to 60 s) was set automatically by the system to reach the most sensitive setting. Imaging parameters and measurement procedures were kept consistent within and between subjects.

In vivo imaging analysis

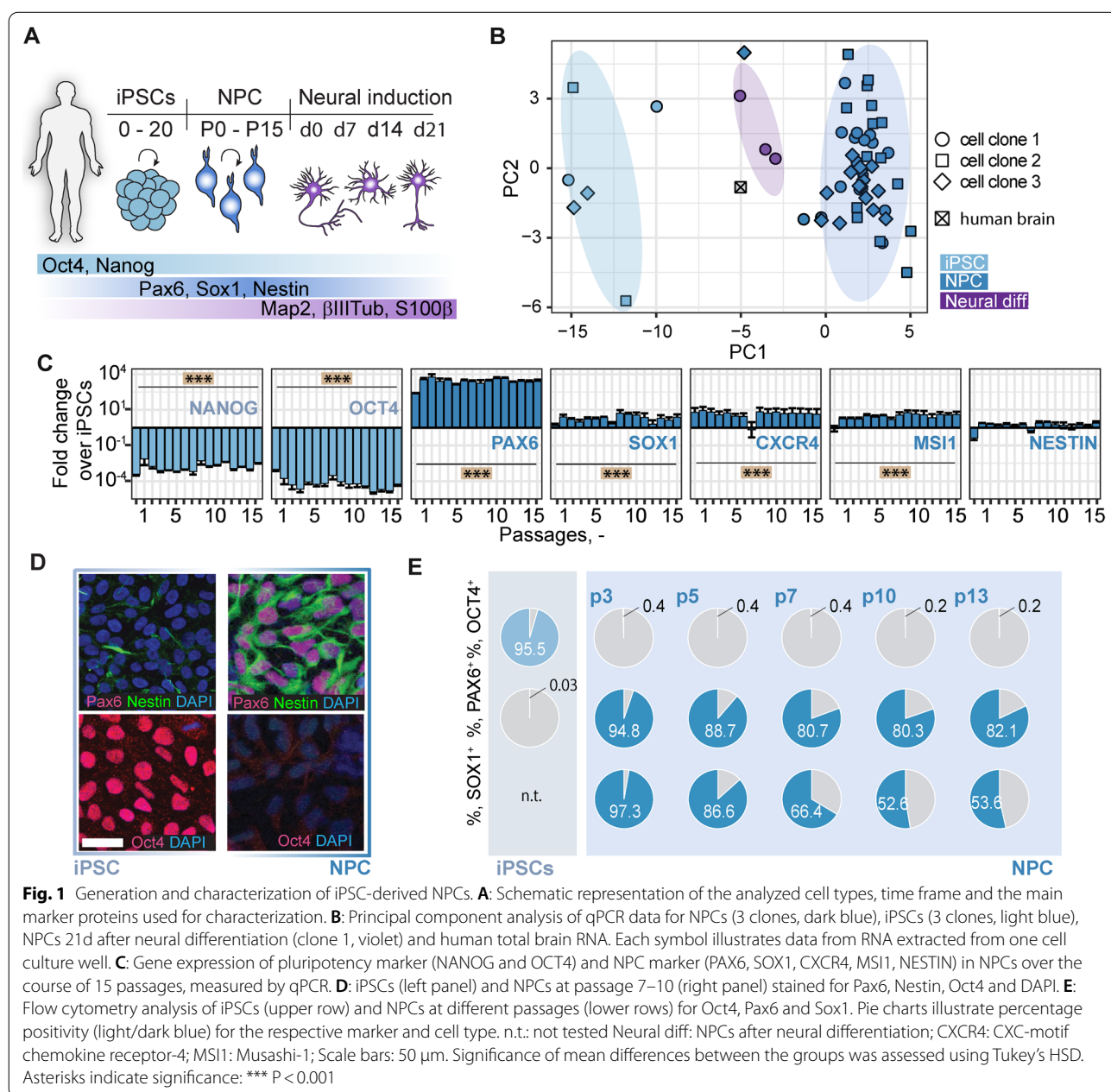
In vivo BLI data was analysed using the Living Image Software (LI 4.7.3) with size-constant ROIs as described before [14, 21]. Briefly, the ROIs were manually drawn based on anatomical landmarks (eyes, ears and snout) on each image. Plotting and statistical analysis were performed using RStudio. The brain-specific signal was

calculated and corrected for nonspecific signal taken from a ROI on the skin of the animal's back and for noise taken from a ROI outside the mouse. Signal-to-noise ratio (SNR) was calculated by dividing the mean photon flux (ph/s/cm²/sr) by the standard deviation of the noise. Bioluminescent signal was calculated by subtracting the background flux from the mean photon flux.

Statistical analysis

Statistical analysis was performed using RStudio 4.0. Sample sizes were designed with adequate power

according to our previous studies. All data were tested for normal distribution by using the Shapiro–Wilk test. Normally distributed data were tested for differences with a two-tailed unpaired one-sample *t*-test to compare changes between two groups (GFP expression of transduced vs. control cells) as in Fig. 4F. Multiple comparisons as in Figs. 1C and Additional file 1: Figure S1A (NPC gene expression differences), Figs. 2B,C,F (protein fluorescence intensity), Fig. 3D (FACS iPSC signal) were initially tested for normal distribution with the Shapiro–Wilk test. The significance of mean differences between



normally distributed multiple comparisons was assessed using Tukey's HSD. Statistical significance was defined as $*p < 0.05$, $**p < 0.01$, and $***p < 0.001$.

Results

Generation of functional, pure iPSC-derived NPCs

To generate human neural cells with a high translational potential we differentiated human iPSCs into neural progenitor cells (NPCs) (Fig. 1A). Differentiation and maintenance of NPCs was carried out using dual-SMAD inhibition, also under xeno- and feeder-free conditions. NPCs were expanded and characterized over at least 15 passages. Gene expression analysis of iPSCs (3 different clones), NPCs (3 different clones) and differentiated cells at 7, 14 and 21 days after neural induction (1 clone) showed cell type- but not clone-specific clustering (Fig. 1B). Human total brain samples clustered next to neural cells which were differentiated from NPCs. Gene expression of pluripotency marker NANOG and OCT4 were highly downregulated in NPCs (all $p < 0.001$), while marker for neural progenitors, i.e. PAX6, SOX1, CXCR4, and MSI1 were stably upregulated over 15 passages (all $p < 0.001$, Fig. 1C). In contrast, HAND1 and FOXA2, markers for mesodermal and endodermal lineages, respectively, were not upregulated and remained constantly low even at high passages (Additional file 1: Figure S1). Immunostainings showed NPC positivity for Pax6 and Nestin but not for Oct4, while iPSCs were stained positive for Oct4 but not Pax6 (Fig. 1D). A mild staining was observed for Nestin. These results were supported by flow cytometry analysis over several passages (Fig. 1E). Karyotype analysis at different passages (p5, p8, p12 and p15) showed a stable 44,XX karyotype (Additional file 2: Figure S2). The NPC differentiation protocol was further tested in two other iPSC clonal lines which gave similar results indicating robust NPC differentiation (Additional file 3: Figure S3).

To determine the spontaneous neural differentiation potential of the generated NPCs, we withdrew CHIR99021, SB431542, hLIF and FGF2 from the NSMM over the course of 3 weeks. Immunocytochemical analysis of differentiated neural cells showed expression of neuronal markers Map2 and β III-Tubulin, astrocyte marker S100 β as well as NPC marker Pax6 but not pluripotency marker Oct4 (Fig. 2A upper row). The punctate staining of vesicular glutamate transporter (vGlut) and vesicular GABA transporter (vGat) along the neurites indicated the formation of synaptic contracts between neurons. Further, the number of β III-Tubulin positive neurites (Fig. 2A, lower row) as well as the fluorescence intensity of Map2 and doublecortin (DCX, Fig. 2B) increase over time (all $p < 0.001$) suggesting a gradual increase in neural cell number and network complexity during differentiation. Compared to undifferentiated NPCs, differentiated cells showed a time-dependent increase in synaptic gene expression (vGAT: all $p < 0.001$; vGLUT: $p < 0.05$ (d14, d21)) (Fig. 2C). Astrocytic genes APOE and S100 β were also partially upregulated (APOE: all $p < 0.001$, S100 β : d14: $p < 0.001$); and while the levels of oligodendrocyte marker slightly increased at d21 it did not reach significance (all $p > 0.05$). Elevated levels of BRN2 and FOXG1 suggested the presence of excitatory cortical neurons. To confirm that differentiated neural cells were active and reacted to stimulation, we expressed mRuby2 and the calcium sensor GCaMP6s under the human synapsin 1 promoter using adeno-associated virus (AAV) (Fig. 2D). Expression of mRuby was only observed in differentiated neural cells but not in undifferentiated NPCs ($p < 0.001$, Fig. 2E, F) indicating activity of the synapsin 1 promoter only in differentiated cells. Neural cells showed higher GCaMP6s signals already at baseline and addition of 60 mM KCl immediately increased GCaMP6s

(See figure on next page.)

Fig. 2 Neural differentiation of NPCs. **A:** Differentiated NPCs, at d21 after differentiation (upper row), stained for Oct4, Pax6, Map2, β III-Tubulin, vGlut and vGat. Differentiated NPCs, at d0, d7, d14 and d21 after differentiation (lower row), stained for β III-Tubulin. **B:** Quantification of fluorescence intensity of microscopy images of differentiated NPCs at d0, d7, d14 and d21 of differentiation, stained for Dcx, S100 β , Map2 and β III-Tubulin. **C:** Gene expression of neuronal (vGAT, vGLUT, BRN2, FOXG1), astrocyte (APOE, S100 β) and oligodendrocyte marker (OLIG2) in differentiated NPCs at 7, 14 and 21 d after neural differentiation, measured by qPCR. Total human brain RNA served as control. **D:** Experimental setup for determining the activity of differentiated NPCs and AAV construct for the expression of GCaMP6s and mRuby under the human synapsin promoter. **E:** Human synapsin promoter-based expression of mRuby in NPCs and differentiated neural cells. Confocal images of NPCs transduced with the AAV-mRuby construct (left), differentiated NPCs at d21 after differentiation (middle) and differentiated NPCs at d21 after differentiation and transduced with AAV-mRuby construct (right). **F:** Quantification of mRuby signal in transduced NPCs (left), non-transduced differentiated neural cells (middle) and transduced neural cells (right) from Fig. 1G. **G:** Confocal time-lapse images of non-transduced, differentiated neural cells (upper row) and neural cells transduced with AAV-GCaMP6s construct (middle row). After 350 s, cells were treated with 60 mM KCL (lower row). Scale bars: 50 μ m. **H:** Quantification of GCaMP6s signal intensity from confocal time-lapse images. vGAT Vesicular GABA Transporter, vGLUT vesicular glutamate transporter, Dcx doublecortin, β IIITub β III-Tubulin, hSyn human synapsin. Boxplots indicate the 25–75% quartiles of the data. Each dot in the plots represents one cell culture well and significance of mean differences between the groups was assessed using Tukey's HSD. Line graphs are plotted as mean \pm sem. Asterisks indicate significance: * $p < 0.05$, ** $p < 0.01$, *** $p < 0.001$

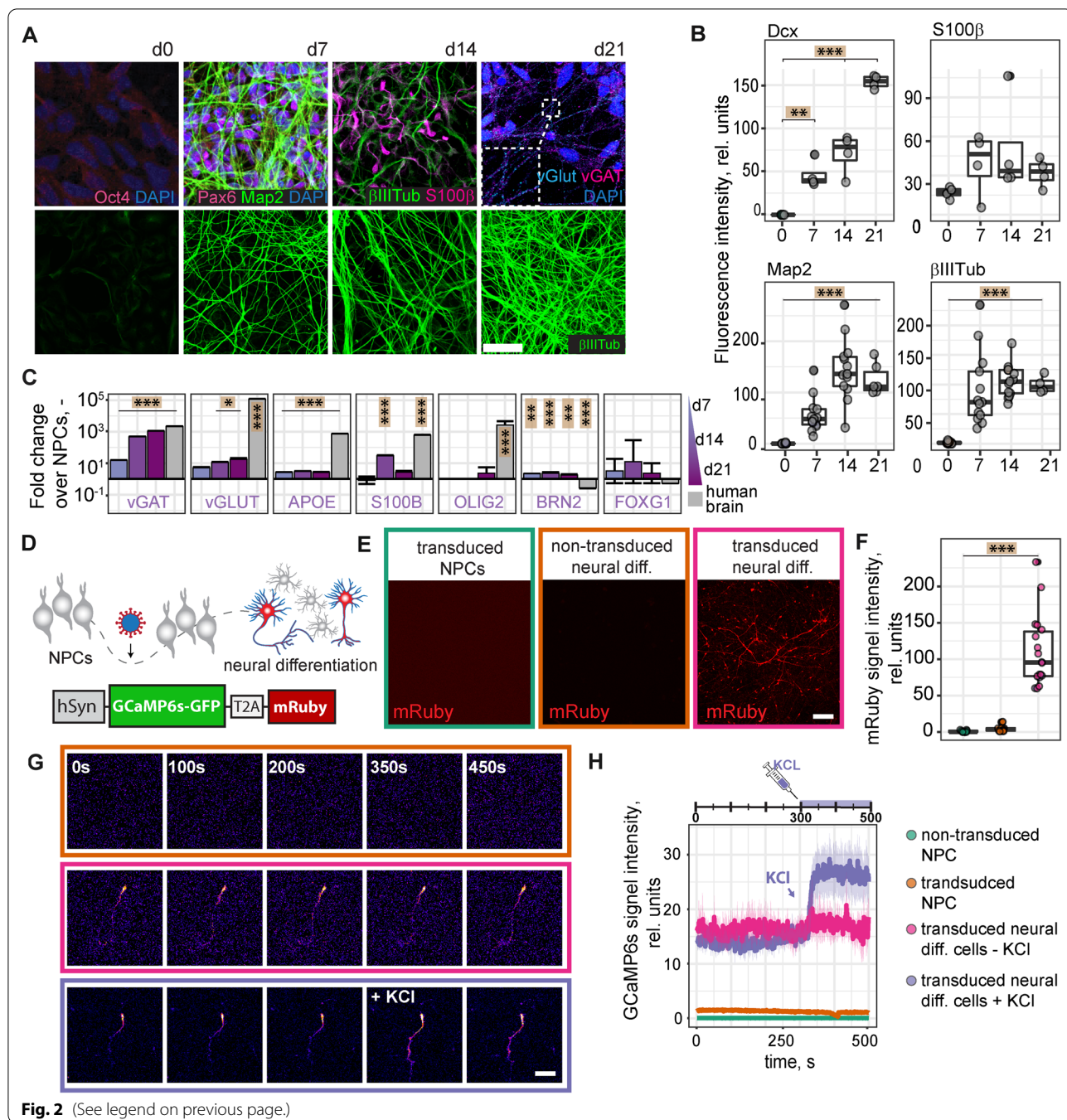


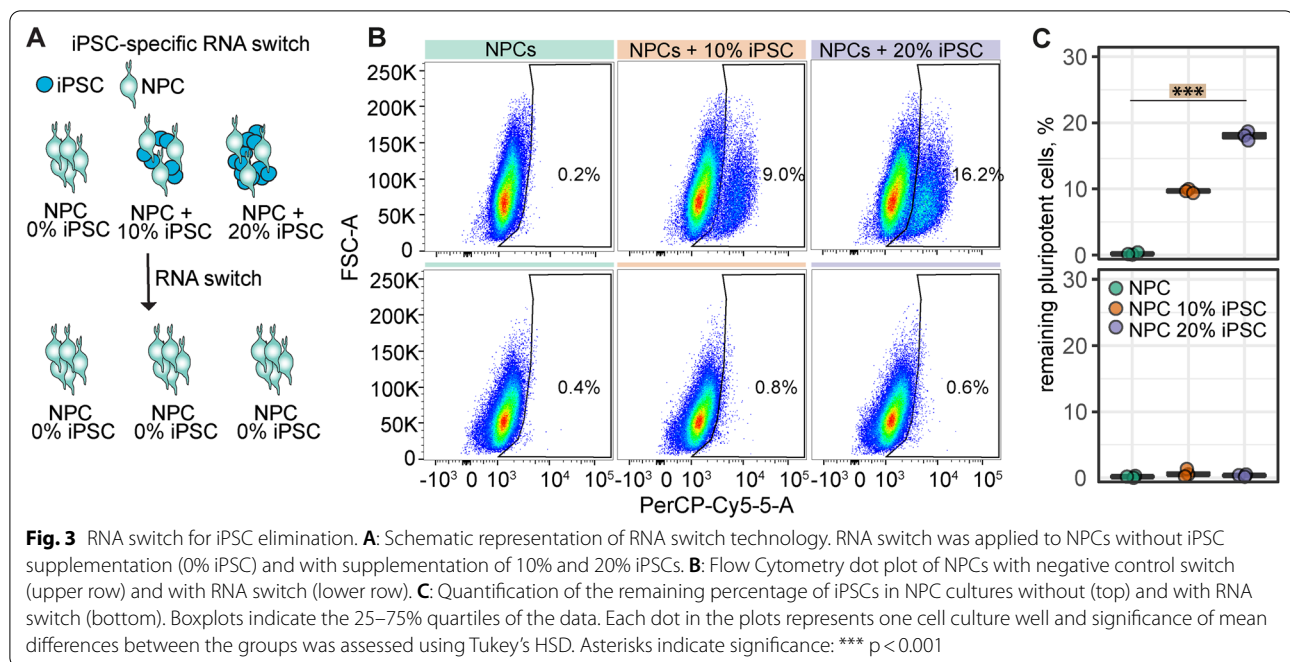
Fig. 2 (See legend on previous page.)

fluorescence, analyzed by confocal live imaging (Fig. 2G, H).

Taken together, iPSC-derived NPCs generated under xeno-free conditions showed i) upregulation of typical NPC markers, ii) strong downregulation of pluripotency markers and iii) spontaneous differentiation into functional neurons and glial cells in vitro.

iPSC-elimination using RNA switch

Remaining pluripotent cells are a major concern for iPSC-based cell therapies. To reduce the risk of iPSC residuals, we took advantage of the RNA switch technology to eliminate potential residual iPSCs. The RNA switch was designed to specifically detect miR-302a-5p that is highly expressed in hiPSCs and eliminate iPSCs in cell cultures



[8, 12, 22]. Since our differentiation protocol already generated a highly pure population of NPCs, we tested the efficacy of the mRNA switch by adding 10% and 20% of iPSCs to the NPC cultures (Fig. 3A). Under both conditions we were able to reduce the iPSC-content of our cultures to $<1\%$ of Oct4-positive iPSCs, as detected by flow cytometry. A negative control RNA switch, in which cells were lipofected with no RNA, did not affect the amount of added iPSCs (Fig. 3 B, C).

Functionalization of NPCs for in vivo tracking

To be able to track NPCs after transplantation, we established a dual-reporter system combining a fluorescence (GFP) and a bioluminescence (red firefly luciferase (rfLuc)) reporter. We determined the optimal expression conditions and tested luminescence signal intensity for three commonly used promoters, i.e. human phosphoglycerate kinase (hPGK), cytomegalovirus (CMV) and human elongation factor 1 alpha (EF1 α) promoter (Fig. 4A). Luminescence signal increased linearly to exposure time, virus titer as well as to the substrate (d-Luciferin) concentration (Fig. 4B, C). The strongest luminescence signals in NPCs were observed when rfLuc was expressed under the EF1 α promoter while CMV gave the lowest signal (Fig. 4D). This is in contrast to HEK cells, in which CMV-driven rfLuc expression resulted in the strongest luminescence signal, indicating that the promoter has to be selected according to the used cell type. For the following experiments, NPCs transduced with the lentiviral dual reporter under the EF1 α promoter

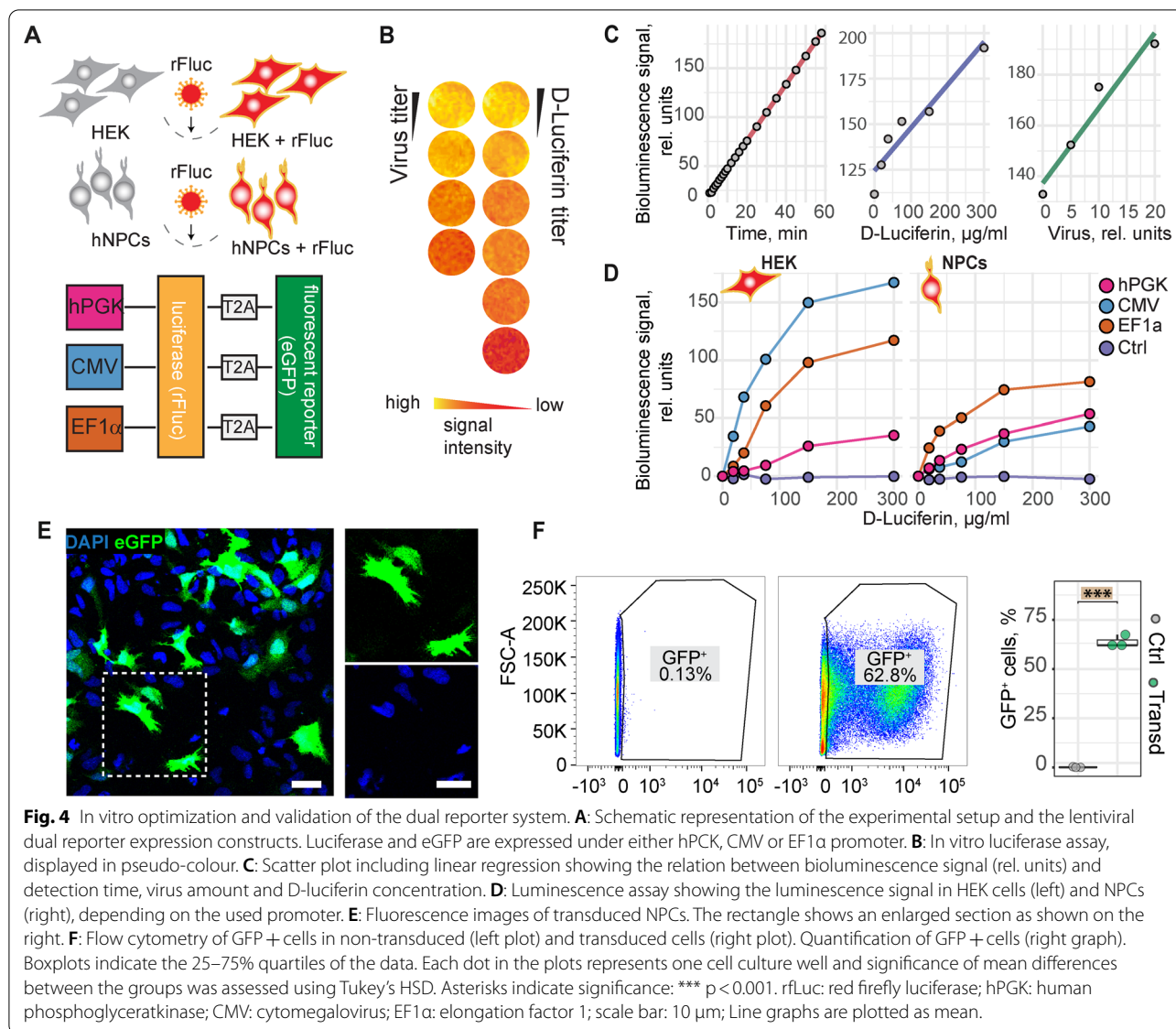
were used with a transduction efficiency of $\sim 60\text{--}70\%$ (Fig. 4E, F).

Transplantation and tracking of NPCs in vivo

For in-depth in vivo characterization of the NPCs, we transplanted 1.6×10^5 cells stereotactically into the right cortex (AP: +0.5 mm, ML: +1.5 mm, DV: -0.8 mm relative to bregma) of wt mice and genetically immunosuppressed NSG or Rag2 $^{-/-}$ mice.

As we used freshly thawed cells for transplantation and transplanting various animals can be time-consuming, it was of high importance to make sure that NPC viability was stable for several hours after thawing and before transplantation. Thus, we analyzed the viability of NPCs after thawing over time. NPCs were thawed, kept on ice for 24 h and cell viability was measured using the Vi-Cell XR Cell Viability Analyzer at various time points. Viability slightly declined during the first 10 h after thawing but remained constant at $>75\%$ for further 14 h (Additional file 4: Figure S4).

To determine the minimum cell number that can be detected by bioluminescence imaging (BLI) in vivo, serial dilutions (2×10^5 , 1×10^5 , 6×10^4 , 1.2×10^4 , 6×10^3 , 2×10^3) of NPCs were transplanted and imaged using bioluminescence imaging. Remarkably, even the lowest cell number transplanted, 2×10^3 NPCs, was detectable (Fig. 5A). A linear relation between bioluminescence signal and transplanted cell number was observed with $R^2 = 0.98$ (Fig. 5B).



Survival of dual reporter-expressing NPCs was analysed throughout a 35d time course in wt and NSG mice. While the BLI signal was constantly reduced over time in wt mice and completely decayed between d12 and d21,

the BLI signal in NSG mice increased until it reached a plateau between d21 and d35 (Fig. 5C, D). This suggests that immunosuppression is essential for the survival of grafted human NPCs.

(See figure on next page.)

Fig. 5 Analysis and in vivo tracking of transplanted NPCs. **A:** Bioluminescence of rFluc-expressing NPCs, transplanted at different numbers into the brain of C57/Bl6 mice at 1.5 h post transplantation. **B:** Scatter plot including linear regression showing the relation between the bioluminescence signal and the number of transplanted cells. **C:** Bioluminescence of rFluc-expressing NPCs, transplanted into NSG (upper row) and C57/Bl6 mice (lower row), over the course of 35d, measured by in vivo bioluminescence imaging. 1.6×10^5 cells have been transplanted. **D:** BLI signal intensity over time (mean \pm SEM per strain, SBR). **E:** Bioluminescence of rFluc-expressing NPCs, transplanted into stroked Rag2 $^{-/-}$ mice. **F:** BLI signal intensity over time (mean \pm SEM per strain, SBR). **G:** Representative histological stainings of transplanted NPCs, 35d post transplantation in stroked Rag2 $^{-/-}$ mice. Arrowheads indicate GFP-expressing cells that are negative for the respective marker. Arrows indicate positivity for marker and GFP. Scale bar = 50 μ m. **H:** Quantification of cells positive for the respective marker and for GFP. BLI bioluminescence imaging, SNR Signal-to-noise ratio, WT wild-type, NSG: NOD scid gamma. Line graphs are plotted as mean \pm sem

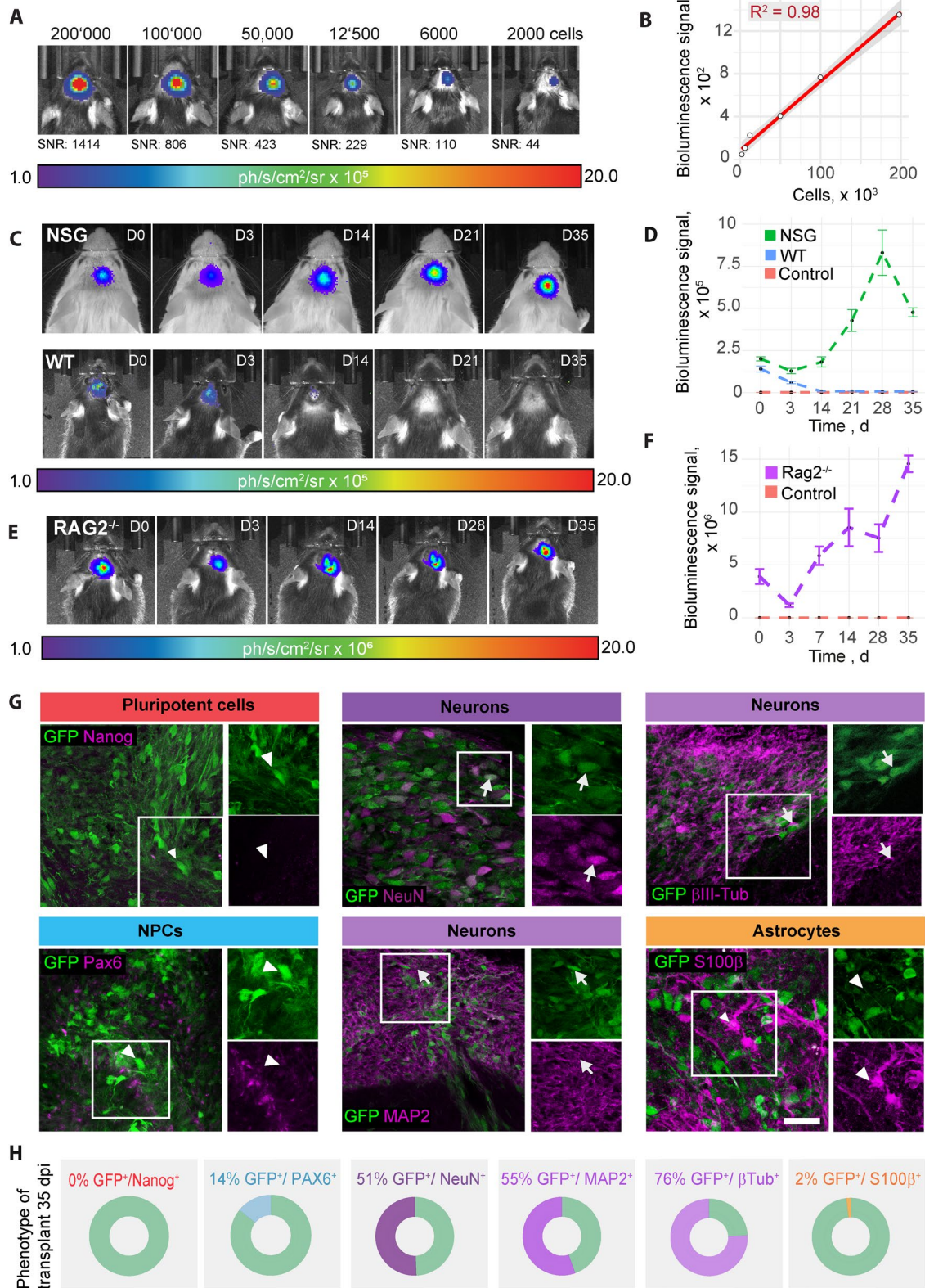


Fig. 5 (See legend on previous page.)

To mimic a more clinically relevant scenario, we stereotactically transplanted rFluc-eGFP NPCs in the ischemic brain of stroked Rag2^{-/-} mice. The stroke volume was approximately 1 mm³ at 42 days post injury (Additional file 5: Figure S5). We confirmed a 35 day long-term survival of the graft using bioluminescence imaging, similar to uninjured animals (Fig. 5E, F).

To assess the long-term differentiation profile of grafted NPCs, we histologically characterized the phenotype of NPCs at 35 days following transplantation in stroked mice. The majority of transplanted GFP⁺ cells expressed various markers of neuronal fate (55% Map2, 76% β III-Tubulin; 51% NeuN) (Fig. 5G, H). While 14% of transplanted GFP⁺ cells still expressed the neural progenitor marker Pax6, only 2% of cells were positive for astrocyte marker S100 β . Importantly, no Nanog-positive cells were detectable at 35 days following transplantation. Hematoxylin–eosin (HE) stained frozen sections (coronal sections of the cortex at the site of engraftment) were examined. They confirmed the presence of a monomorphic population of small cells with ovoid nuclei and sparse cytoplasm. Mitotic figures were not observed, and there was no evidence of necrosis, an inflammatory reaction or distinct stroma or new vessel formation (Additional file 6: Figure S6). Further, co-staining of grafted cells with anti Ki67 (marker for proliferating cells) and anti human nuclei (HuNu; marker for grafted human cells) antibodies showed only 1% double-positive cells, indicating a very low proliferation rate (Additional file 7: Figure S7). Few endogenous (Hunu-negative) proliferating cells were also observed. These findings are consistent with an absence of neoplastic transformation and growth.

In sum, we generated highly pure NPCs from xeno-free iPSCs. These cells can be longitudinally tracked in vivo and identified in the brain sections using a dual reporter system. The NPCs have the capability to spontaneously differentiate into functional neurons in vitro and in vivo.

Discussion

Despite the high prevalence of neurodegenerative diseases and brain injuries, clinical therapies remain limited. Advances in iPSC technology have brought cell therapy back into the focus of treatment options for the brain [5]. Here, we describe the generation of iPSC-derived NPCs for in vivo applications. By modification of previously established monolayer protocols [10, 23] we generated highly scalable NPC cultures—yielding 10¹⁸ NPCs after 15 passages when starting from 10⁶ iPSCs—which are xeno-free and chemically defined. Therefore, this simple monolayer protocol, which does not require cell selection or purification,

can smoothly be adapted to GMP-grade for clinical applications. This is of high importance as changes in media composition or in the cell coating during transition from research-grade to a GMP-compliant clinical-grade cell production can strongly affect iPSC differentiation potential and the characteristics of the resulting cells which would complicate the potential clinical translation. We differentiated three iPSC clonal lines to NPCs and showed comparable expression levels of classical NPC marker proteins among all lines. Gene expression analysis revealed a cell type-dependent clustering, clearly distinguishing between iPSCs, NPCs and neural cells while no cell clone-based clustering was observed in NPCs. While typical NPC markers were increased, mRNA levels of other cell lineages markers, i.e. meso- and endoderm, remained low over all passages, indicating a stable NPC identity. To determine the potential of NPCs to spontaneously differentiate into neural cells, we withdrew GSK-3 β inhibitor CHIR99021, TGF- β inhibitor SB431542, hLIF and FGF2 from the stem cell maintenance medium and cultured the cells for 4 weeks. We found that cells slowed down their proliferation and differentiated into neurons, astrocytes and oligodendrocytes. Expression of calcium sensor GcAMP6 under the human synapsin promoter showed that cells were active and reacted to KCl stimulation indicating the differentiation into functional neuronal cultures. Gene expression analysis further showed a close clustering of differentiated neural cells to human brain lysate, confirming the high translational aspect of iPSC-derived NPCs.

Besides scalability, another crucial point of cell therapy is the purity of the differentiated cells. Residual pluripotent cells in the therapeutic product can cause teratoma formation [5]. The risk for tumours can be strongly reduced by applying highly efficient differentiation and purification protocols. While the differentiation of the iPS cell lines in this study was very effective, evidenced by a strong reduction in pluripotent genes and $\leq 0.4\%$ Oct4-positive cells in the NPC culture, it cannot be excluded that other iPS cell lines may not yield such a high purity when differentiated to NPCs. Therefore, we tested the compatibility of the obtained NPCs with synthetic RNA switches, a state-of-the-art cell purification technique. The RNA switch technology is a powerful tool for enriching or eliminating a specific cell type in a mixed culture [24]. When we added iPSCs to the NPC culture (10–20%), the RNA switch resulted in the elimination of iPSCs back to baseline signal. Importantly, when we applied the RNA switch to our NPCs without iPSC addition, we did not observe a difference—flow cytometry still showed 0.2–0.4% Oct4-positive cells. This

indicates that the NPC cultures used in this study are already so pure that the RNA switch technique does not have to increase its purity further. Accordingly, we did not observe signs of tumour formation *in vivo*, 4 weeks after transplantation.

An increasing number of studies recently reported the production of NPCs or neural stem/progenitor cells (NSPCs) from either embryonic stem cells or from iPSCs using GMP-compatible techniques [7, 25–27]. The first-in-man study using iPSC-derived NSPCs for the treatment of spinal cord injury is currently in preparation at Keio University Hospital, Tokyo, Japan [27]. A further trial is currently performed with iPSC-derived dopaminergic precursor cells to treat Parkinson's Disease [28]. As most clinical strategies rely on allogeneic cell therapies (cells are derived from a healthy donor), iPSC-based therapies will require general immunosuppression for a prolonged period, e.g. with Tacrolimus to inhibit T cell activation [16, 28].

While many NPC differentiation protocols are laborious and tedious, and require embryoid body formation, neural rosette-selection or colony-picking [7, 25–27], the protocol applied here is simply based on a monolayer culture and the treatment with defined neural induction media. A further limitation of several studies, which applied NPSc *in vivo*, is the dependence on endpoint-measures due to the lack of appropriate long-term *in vivo* imaging techniques of graft survival. To circumvent this issue, we used lentiviral-mediated expression of a dual-reporter consisting of rFluc and eGFP, which allowed the *in vivo* tracking of the cell graft via bioluminescence imaging as well as the identification of the grafted cells in brain slices through the eGFP signal. The comparison of different promoters showed that EF1 α gave the highest luminescence signal in NPCs while CMV-mediated expression was lowest. Interestingly, this was opposed to our findings in HEK cells indicating that different cell types have different promoter activities. This finding is in accordance with previous observations showing that stem cells can silence exogenous promoters such as CMV [29].

Although we reached a high sensitivity and strong signals during *in vivo* bioluminescence imaging, it was not possible to resolve local cell migration in adjacent brain regions. Furthermore, the bioluminescence signal of other cell types/cell lines may vary due to differences in promoter strength or luciferin metabolism. Detection of cells may also become more challenging in experimental set-ups that require intravenous/systemic injections of cells because of the expected low transmissibility at the blood brain barrier (BBB). These effects may be less pronounced in neurodegeneration

or brain injury patients and animal models that are usually associated with BBB damage and increased permeability [19, 30]. Furthermore, we focused in this study on the engraftment and phenotyping of the transplanted cells in healthy and stroked mice. We did not perform behavioural experiments and did not assess whether the transplanted cells contributed to improved functional recovery. However, the functional benefits of cell therapy after experimental stroke have been described thoroughly before [31–33].

For our study, we engrafted freshly thawed NPCs, without the need of taking the cells into culture before transplantation. Thus, these cells represent a potential off-the-shelf product for cell transplantation. Cell survival in C57/BL6 mice strongly dropped 14 days post transplantation, while the signal increased in non-injured and in stroked immunodeficient mice. This suggests that the transplanted human cells were attacked by the immune system in non-immunosuppressed mice. It further shows that grafted NPCs survive even in the hostile environment of an ischemic stroke. To exclude that the increased bioluminescent signal in NSG mice is caused by tumour formation, we analyzed histological brain sections. We did not find evidence of tumour formation in histological sections. In contrast, most eGFP-positive, grafted NPCs differentiated into neurons, evidenced by the high positivity for the neuronal markers NeuN, MAP2 and β III-Tubulin. Therefore, we conclude that the increase in bioluminescence signal is either due to an increased expression in the differentiated cells and/or due to the larger area that neurons cover compared to the smaller NPCs.

Most NPCs, that we transplanted into the stroked mouse brain, differentiated into neurons and only 2% of cells were positive for astrocyte markers. Several *in vitro* studies have shown that oxygen levels contribute to determining the ratio of neurons and astrocytes, differentiated from NPCs. While 20% oxygen generated a 3:1 ratio of neurons to astrocytes, derived from iPSC-NPCs [34], an increase in the fraction of astrocytes was observed under hypoxic conditions [35, 36]. This stands in contrast to the low number of astrocytes generated from the NPCs grafted into the stroked mouse brain in our study. However, reducing oxygen levels in cell culture may not fully mimic the complex environment and the conditions that the graft is exposed to in the stroked brain. Thus, it will be interesting to determine how hypoxic conditions *in vitro* and *in vivo* affect the differentiation potential of our NPCs. Further, follow-up studies are required to determine whether the grafted cells functionally integrate into the neural network and can induce functional recovery in the stroked mice.

Conclusions

Taken together, we report the production of xeno-free human NPCs which can be functionalized to allow non-invasive in vivo tracking of the graft over time. After 1 months, engrafted cells mainly displayed a neuronal phenotype with some NPCs remaining. No signs of tumour formation were found. This simple differentiation protocol combined with the ability of in vivo cell tracking presents a valuable tool to develop safe and effective cell therapies for brain injuries.

Supplementary Information

The online version contains supplementary material available at <https://doi.org/10.1186/s12967-022-03610-5>.

Additional file 1: Figure S1. Expression of different cell lineage markers in NPCs. Gene expression of markers for ectodermal (PAX6), mesodermal (HAND1) and endodermal (FOXA2) cell lineages, as well as for pluripotent cells (NANOG and OCT4), in iPSCs and NPCs from three clonal lines at different passages, measured by qPCR. Boxplots show –CT values.

Additional file 2: Figure S2. NPC karyotype. Q-banding karyotype of NPCs at different passages.

Additional file 3: Figure S3. Characterization of iPSC-derived NPCs from two other iPSC clonal lines. A: Gene expression of pluripotency marker (NANOG and OCT4) and NPC marker (PAX6, SOX1, CXCR4) in NPCs from iPSC clonal lines 2 (upper row) and 3 (lower row) over the course of 15 passages, measured by qPCR. B: Flow cytometry analysis of iPSCs (upper row) and NPCs from iPSC clonal lines 2 and 3 at different passages for Oct4, Pax6 and Sox1. Pie charts illustrate percentage positivity (light/dark blue) for the respective marker and cell type. n.t.: not tested.

Additional file 4: Figure S4. Cell viability in vitro. Percentage of freshly thawed viable NPCs over the time course of 25h on ice, measured using Vi-Cell XR Cell Viability Analyzer.

Additional file 5: Figure S5. Lesion size. Quantification of stroke area (plotted as mean \pm sem) and stroke volume at 42 dpi. Boxplots indicate the 25% to 75% quartiles of the data.

Additional file 6: Figure S6. HE staining. HE staining of the stroked mouse brain, 35d after NPC transplantation. red: stroked hemisphere; green: contralesional, intact hemisphere; black: area of cell transplantation

Additional file 7: Figure S7. Quantification of proliferating cells. A: Representative histological staining of transplanted NPCs against proliferation marker Ki67 (blue) and human nuclei (green; grafted cells), 35d post transplantation in stroked Rag2^{-/-} mice. Arrowheads indicate Ki67-expressing cells that are negative for HuNu. B: Quantification of cells positive for HuNu and Ki67.

Additional file 8: Table S1. Detailed list of cell culture media and substances.

Additional file 9: Table S2. qPCR primer list.

Acknowledgements

We thank Dr. Yoshihiko Fujita, Center for iPS Cell Research and Application (CiRA), Kyoto University, Kyoto, Japan, for providing RNA-switch plasmids. We also thank Prof. Anja Kipar, Laboratory for Animal Model Pathology, Institute of Veterinary Pathology, Vetsuisse Faculty, University of Zurich, for the histological examination. We further appreciate the help of Sarina Seiter, Institute for Regenerative Medicine, University of Zurich, for karyotype analysis and the Institute for Medical Genetics for using their lab equipment.

Author contributions

Ruslan Rust: Conception and design, Financial support, Collection and/or assembly of data, Data analysis and interpretation, Manuscript writing, Approval of manuscript. *Rebecca Weber*: Conception and design, Collection

and/or assembly of data, Data analysis and interpretation, Manuscript writing, Approval of manuscript. *Melanie Generali*: Conception and design, Collection and/or assembly of data, Data analysis and interpretation, Approval of manuscript. *Debora Kehl*: Collection and/or assembly of data, Data analysis and interpretation, Approval of manuscript. *Chantal Bodenmann*: Conception and design, Collection and/or assembly of data, Data analysis and interpretation, Approval of manuscript. *Daniela Uhr*: Conception and design, Collection and/or assembly of data, Data analysis and interpretation, Approval of manuscript. *Debora Wanner*: Conception and design, Collection and/or assembly of data, Data analysis and interpretation, Approval of manuscript. *Kathrin Zürcher*: Conception and design, Collection and/or assembly of data, Data analysis and interpretation, Approval of manuscript. *Hirohide Saito*: Provision of material, Approval of manuscript. *Simon P. Hoerstrup*: Conception and design, Financial support, Approval of manuscript. *Roger M. Nitsch*: Conception and design, Financial support, Approval of manuscript. *Christian Tackenberg*: Conception and design, Financial support, Collection and/or assembly of data, Data analysis and interpretation, Manuscript writing, Approval of manuscript. All authors read and approved the final manuscript.

Funding

The authors acknowledge funding from Mäxi Foundation, Swiss 3R Competence Center (OC-2020–002) and the Swiss National Science Foundation (CRSK-1_195902).

Availability of data and materials

All raw data are available upon request from the corresponding authors.

Declarations

Ethics approval and consent to participate

The use of human iPSC lines was approved by the Zurich Cantonal Ethics Committee (Approval Nr.: 2014–0430). Animal experiments were performed in accordance with governmental and institutional (University of Zurich) guidelines and have been approved by the Cantonal Veterinary Office of Zurich (License number: 31687).

Consent for publication

Not applicable.

Competing interests

Hirohide Saito owns shares and is outside director of aceRNA Technologies, Ltd.

Author details

¹Institute for Regenerative Medicine, University of Zurich, Wagistrasse 12, 8952 Schlieren, Switzerland. ²Neuroscience Center Zurich, University of Zurich and ETH Zurich, Zurich, Switzerland. ³Wyss Translational Center Zurich, University and ETH Zurich, Zurich, Switzerland. ⁴Department of Life Science Frontiers, Center for iPS Cell Research and Application (CiRA), Kyoto University, Kyoto, Japan.

Received: 3 May 2022 Accepted: 24 August 2022

Published online: 16 September 2022

References

- Rust R, Grönnert L, Weber RZ, Mulders G, Schwab ME. Refueling the Ischemic CNS: Guidance Molecules for Vascular Repair. *Trends Neurosci.* 2019;42(9):644–56.
- Naggal A, Choy FC, Howell S, Hillier S, Chan F, Hamilton-Bruce MA, et al. Safety and effectiveness of stem cell therapies in early-phase clinical trials in stroke: a systematic review and meta-analysis. *Stem Cell Res Ther.* 2017;8(1):191.
- Borlongan CV. Concise Review: Stem Cell Therapy for Stroke Patients: Are We There Yet? *Stem Cells Transl Med.* 2019;8(9):983–8.
- Duan R, Gao Y, He R, Jing L, Li Y, Gong Z, et al. Induced Pluripotent Stem Cells for Ischemic Stroke Treatment. *Front Neurosci.* 2021;15: 628663.
- Yamanaka S. Pluripotent Stem Cell-Based Cell Therapy—Promise and Challenges. *Cell Stem Cell.* 2020;27(4):523–31.

6. Fusaki N, Ban H, Nishiyama A, Saeki K, Hasegawa M. Efficient induction of transgene-free human pluripotent stem cells using a vector based on Sendai virus, an RNA virus that does not integrate into the host genome. *Proc Jpn Acad Ser B Phys Biol Sci*. 2009;85(8):348–62.
7. Bohaciakova D, Hruska-Plochan M, Tsunemoto R, Gifford WD, Driscoll SP, Glenn TD, et al. A scalable solution for isolating human multipotent clinical-grade neural stem cells from ES precursors. *Stem Cell Res Ther*. 2019;10(1):83.
8. Parr CJ, Katayama S, Miki K, Kuang Y, Yoshida Y, Morizane A, et al. MicroRNA-302 switch to identify and eliminate undifferentiated human pluripotent stem cells. *Sci Rep*. 2016;9(6):32532.
9. Miki K, Endo K, Takahashi S, Funakoshi S, Takei I, Katayama S, et al. Efficient Detection and Purification of Cell Populations Using Synthetic MicroRNA Switches. *Cell Stem Cell*. 2015;16(6):699–711.
10. Sancho-Martinez I, Nivet E, Xia Y, Hishida T, Aguirre A, Ocampo A, et al. Establishment of human iPSC-based models for the study and targeting of glioma initiating cells. *Nat Commun*. 2016;22(7):10743.
11. Birnbaum JH, Wanner D, Gietl AF, Saake A, Hock C, Nitsch RM, et al. Oxidative stress and altered mitochondrial protein expression in the absence of amyloid-beta and tau pathology in iPSC-derived neurons from sporadic Alzheimer's disease patients. *Stem Cell Research*. 2018;27:121–30.
12. Fujita Y, Hirokawa M, Hayashi K, Hatani T, Yoshida Y, Yamamoto T, Saito H. A versatile and robust cell purification system with an RNA-only circuit composed of microRNA-responsive ON and OFF switches. *Sci Adv* 2022. <https://doi.org/10.1126/sciadv.abj1793>
13. Weber RZ, Mulders G, Perron P, Tackenberg C, Rust R. Molecular and anatomical roadmap of stroke pathology in immunodeficient mice. *bioRxiv*. 2022. <https://doi.org/10.1101/2022.07.28.501836>.
14. Weber RZ, Bodenmann C, Uhr D, Zürcher KJ, Wanner D, Nitsch RM, et al. Intracerebral Transplantation and In Vivo Bioluminescence Tracking of Human Neural Progenitor Cells in the Mouse Brain. *J Vis Exp*. 2022. <https://doi.org/10.3791/63102>.
15. Kelly S, Bliss TM, Shah AK, Sun GH, Ma M, Foo WC, et al. Transplanted human fetal neural stem cells survive, migrate, and differentiate in ischemic rat cerebral cortex. *Proc Natl Acad Sci*. 2004;101(32):11839–44.
16. Rust R, Tackenberg C. Stem cell therapy for repair of the injured brain: Five principles. *Neuroscientist*. 2022. <https://doi.org/10.1177/10738584221110100>.
17. Rust R, Grönnert L, Gantner C,ENZler A, Mulders G, Weber RZ, et al. Nogo-a targeted therapy promotes vascular repair and functional recovery following stroke. *Proc Natl Acad Sci U S A*. 2019;116(28):14270–9.
18. Rust R, Weber RZ, Grönnert L, Mulders G, Maurer MA, Hofer AS, et al. Anti-Nogo-a antibodies prevent vascular leakage and act as pro-angiogenic factors following stroke. *Sci Rep*. 2019;9(1):20040.
19. Weber RZ, Grönnert L, Mulders G, Maurer MA, Tackenberg C, Schwab ME, et al. Characterization of the blood brain barrier disruption in the photo-thrombotic stroke model. *Front Physiol*. 2020;11: 586226.
20. Weber RZ, Mulders G, Kaiser J, Tackenberg C, Rust R. Deep learning based behavioral profiling of rodent stroke recovery. *Biorxiv*. 2021. <https://doi.org/10.1101/2021.08.11.455647v1>.
21. Aswendt M, Adamczak J, Couillard-Despres S, Hoehn M. Boosting bioluminescence neuroimaging: an optimized protocol for brain studies. *PLoS ONE*. 2013;8(2): e55662.
22. Nakanishi H, Saito H. Purification of specific cell populations differentiated from stem cells using microRNA-responsive synthetic messenger RNAs. *Methods Mol Biol*. 2021;2312:73–86.
23. Li W, Sun W, Zhang Y, Wei W, Ambasadhan R, Xia P, et al. Rapid induction and long-term self-renewal of primitive neural precursors from human embryonic stem cells by small molecule inhibitors. *Proc Natl Acad Sci U S A*. 2011;108(20):8299–304.
24. Karagiannis P, Fujita Y, Saito H. RNA-based gene circuits for cell regulation. *Proc Jpn Acad Ser B Phys Biol Sci*. 2016;92(9):412–22.
25. Vitillo L, Durance C, Hewitt Z, Moore H, Smith A, Vallier L. GMP-grade neural progenitor derivation and differentiation from clinical-grade human embryonic stem cells. *Stem Cell Res Ther*. 2020;11(1):406.
26. Vitillo L, Vallier L. Derivation of Multipotent Neural Progenitors from Human Embryonic Stem Cells for Cell Therapy and Biomedical Applications. In: Turksen K, editor. *Methods in molecular biology*. Clifton NJ: Springer; 2021.
27. Sugai et al., First-in-human clinical trial of transplantation of iPSC-derived NS/PCs in subacute complete spinal cord injury: Study protocol. 2021. *Regen Ther*. <https://doi.org/10.1016/j.reth.2021.08.005>.
28. Takahashi J. iPSC cell-based therapy for Parkinson's disease: A Kyoto trial. *Regen Ther*. 2020;13:18–22.
29. Xia X, Zhang Y, Zieth CR, Zhang SC. Transgenes delivered by lentiviral vector are suppressed in human embryonic stem cells in a promoter-dependent manner. *Stem Cells Dev*. 2007;16(1):167–76.
30. Nation DA, Sweeney MD, Montagne A, Sagare AP, D'Orazio LM, Pachicano M, et al. Blood-brain barrier breakdown is an early biomarker of human cognitive dysfunction. *Nat Med*. 2019;25(2):270–6.
31. Andres RH, Horie N, Slikker W, Keren-Gill H, Zhan K, Sun G, et al. Human neural stem cells enhance structural plasticity and axonal transport in the ischaemic brain. *Brain*. 2011;134(Pt 6):1777–89.
32. Moshayed P, Nih LR, Llorente IL, Berg AR, Cinkornpumin J, Lowry WE, et al. Systematic optimization of an engineered hydrogel allows for selective control of human neural stem cell survival and differentiation after transplantation in the stroke brain. *Biomaterials*. 2016;105:145–55.
33. Wang Y, Zhao Z, Rege SV, Wang M, Si G, Zhou Y, et al. 3K3A-activated protein C stimulates postischemic neuronal repair by human neural stem cells in mice. *Nat Med*. 2016;22(9):1050–5.
34. Patterson M, Chan DN, Ha I, Case D, Cui Y, Handel BV, et al. Defining the nature of human pluripotent stem cell progeny. *Cell Res*. 2012;22(1):178–93.
35. Xie Y, Zhang J, Lin Y, Gaeta X, Meng X, Wisidagama DRR, et al. Defining the role of oxygen tension in human neural progenitor fate. *Stem Cell Rep*. 2014;3(5):743–57.
36. Llorente IL, Xie Y, Mazzitelli JA, Hatanaka EA, Cinkornpumin J, Miller DR, et al. Patient-derived glial enriched progenitors repair functional deficits due to white matter stroke and vascular dementia in rodents. *Sci Transl Med*. 2021;13(590):6747.

Publisher's Note

Springer Nature remains neutral with regard to jurisdictional claims in published maps and institutional affiliations.

Ready to submit your research? Choose BMC and benefit from:

- fast, convenient online submission
- thorough peer review by experienced researchers in your field
- rapid publication on acceptance
- support for research data, including large and complex data types
- gold Open Access which fosters wider collaboration and increased citations
- maximum visibility for your research: over 100M website views per year

At BMC, research is always in progress.

Learn more biomedcentral.com/submissions

